Chap. 11 : Maximally localized rigid unit modes and structural diversity of cristobalite-like crystals

M. Smirnov (1), P. Saint-Grégoire (2)
(1) Physical Department, Saint-Petersburg State University, Russia
(2) CAL (http://co-ac.com), 34110 Frontignan, France
Corresponding author : m.smirnov@spbu.ru

Abstract : It is shown that the particular feature of the ideal β-cristobalite "C9 lattice" (with space group *Fd3m*) is the existence of Chain Tilting Modes (CTM) localized within infinite linear chains of the linked tetrahedra. Within a CTM the tetrahedra forming the chain may concordantly rotate without perturbing the rest of the lattice. It is shown that arbitrary Rigid Unit Mode (RUM) of the C9 structure can be represented as a combination of CTMs. It is also shown that all experimentally determined cristobalite-like crystal structures can be represented as originated from the ideal C9 lattice by a distortion represented as linear combinations of CTMs.

Keywords : SILICA, POLYMORPHISM, RIGID UNIT MODES

Cite this paper: M.B. Smirnov and P. Saint-Gregoire, OAJ materials and Devices, vol 5(1) – chap No11 in "Perovskites and other Framework Structure Crystalline Materials", p 355 (Coll. Acad. 2021) - DOI:10.23647-ca.md20202205

I. Review of the cristobalite-like structures

The family of the cristobalite-like crystal structures is acknowledged to be one of the most representative example of the tetrahedral framework crystal structures (FWS). The family is of particular interest because of its large structural and compositional variety. Such structures known from literature are listed in Table 1. The aristotype of the family is the β-cristobalite. The first determination made by Wyckoff in 1925 [1] declared for the high-temperature cristobalite the cubic *Fd*3*m* (C9) structure with regular SiO_4 tetrahedra and linear Si-O-Si angles (see first column in Table 1). The silicon atoms are arranged in the diamond-like FCC lattice and the oxygen atoms are situated in the middle of the Si-Si contacts (see Figure 1). This is the most symmetric and the most open cristobalite structure.

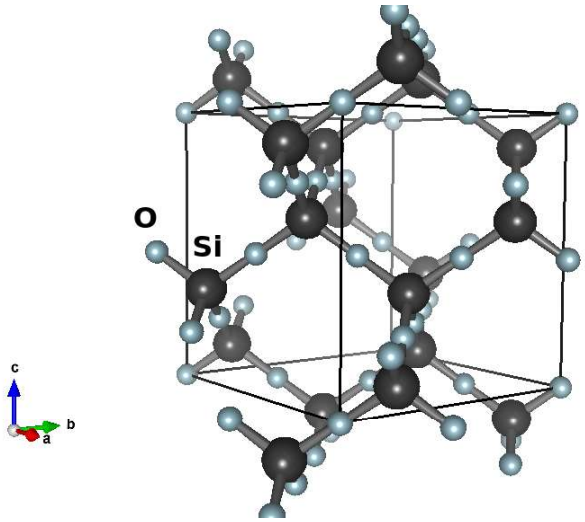

Figure 1: Structure of high cristabolite (C9, cubic *Fd*3*m* symmetry)

Two neighbouring oxygen tetrahedra share one oxygen atom located in the middle of a Si-Si line (From data of ref. [2]).

All other cristobalite-like structures listed in Table 1 can be considered as resulting from distortions which consist of concordant tetrahedron rotations or displacement. Now we briefly discuss all the structures. In fact, the real structure of the high-temperature cristobalite is still debatable. The C9 model proposed by Wyckoff was put in doubts because of unrealistically short Si-O bond lengths. Moreover, further progress in the X-ray scattering technique revealed some reflections prohibited for the C9. Thus, a necessary refinement was proposed in 1932 [3]. Keeping the cubic unit cell with 8 SiO_2 units, all possible space symmetry groups were tested. Finally it was

found that the best agreement gives the $P2_13$ (#198, T_4) structure with O positions slightly shifted from their sites in the ideal C9 structure such as to yield bond distances and angles in the right range.

Table 1: Cristobalite-like collapsed structures, unit cell multiplicity Z, references

	Space group		Z	Compound	Ref.
1	#227	*Fd*3*m*	2	SiO_2	[1,2]
2	#122	$I\bar{4}2d$	2	SiO_2	[4]
3	#92	$P4_12_12$	4	SiO_2	[6]
4	#198	$P2_13$	8	SiO_2	[3]
5	#14	*P*2$_1$/*c*	8	SiO_2	[9]
6	#33	*Pna*2$_1$	4	$NaGaO_2$	[12]
7	#61	*Pbca*	16	$KGaO_2$	[12]
8	#29	*Pb*2$_1$*a*	16	$NaAlSiO_4$	[13]

Alternatively, it was proposed that β-cristobalite has a disordered structure. Disordered structural models have been proposed by Nieuwenkamp [4] and by Wright and Leadbetter [5]. In the model proposed by Nieuwenkamp, the O atoms are randomly distributed over six equivalent sites forming a circle normal to the Si–Si axis such that the cubic *Fd*3*m* symmetry was preserved. In Ref. [5] it was proposed to assign the origin of the six O positions to superposition of six structures with SiO_4 tetrahedra tilted by about ±20° around the three C_4 axis. Each of the six tilted configurations is a tetragonal structure with $I\bar{4}2d$ (#122, D_{2d}^{12}) symmetry (see third line in Table 1). The pseudo-cubic *Fd*3*m* symmetry of the diffraction pattern was supposed to result from the averaging over small D_{2d} domains with different orientations of the tetragonal axis.

The low-temperature cristobalite phase, α-polymorph (see forth line in Table 1) also has a collapsed structure which was identified as a tetragonal one with space symmetry $P4_12_12$ (#92) [6]. This structure can be considered as the result of the RUM condensation [7].

One more polymorph of the cristobalite SiO_2 was revealed in the high-pressure studies. It was found that under hydrostatic compression up to ~ 1.5 GPa the α-cristobalite undergoes a structural phase transition. The high-pressure phase, referred to as cristobalite-II was indexed according to a monoclinic unit cell [8]. The space symmetry group of the structure was determined as $P2_1/c$ (C_{2h}\5, #14) [9]. It was also suggested that the structure of phase-II could arise by a displacive distortion of the cubic β-cristobalite. However, the atomistic pattern of the α-cristobalite → cristobalite-II transformation was not yet reported. Below we shall discuss this question in more details.

The specific feature of the cristobalite structure is the presence of large cavities within the SiO_2 framework. Such cavities form hexagonal channels well observable in the *xyz* projection (see Figure 1). This structural peculiarity gives rise to the existence of the "filled" or "stuffed" cristobalite derivatives, in which some additional cations, typically alkali metals, come into the channels and occupy the interstitial sites [10, 11]. For the charge neutrality conditions, such intercalation is accompanied by partial replacement of the Si^{4+} ions in the cristobalite framework by trivalent ($A1^{3+}$, Ga^{3+}) or divalent (Ca^{2+}, Mg^{2+}) ions. For the first time, such stuffed cristobalite-like structures, $NaAlSiO_4$ and Na_2CaSiO_4, were reported in 1935 [10]. The crystal structure of these compounds was found isomorphic to Barth's #198 structure. Later on, this family was enlarged by inclusion of Fe as the replacing atoms and by intercalation of potassium instead of sodium [11]. Other crystal structures were found for the stuffed cristobalite-like gallates $NaGaO_2$ (#33) and $KGaO_2$ (#61) [12]. Later another cristobalite-like stuffed structure was proposed for the carnegieite $NaAlSiO_4$ (#29) [13]. These structures without intercalates alkali atoms are shown in the lines 6-8 of Table 1. It can be shown that the oxy-tetrahedron frameworks of all these structures can be represented as RUM-distorted C9 structures.

It is noticeable that the cristobalite-like structures shown in Table 1 are widely spread in nature. Besides silica, other oxides of the IV group elements crystallize in the cristobalite-like polymorphs, such as GeO_2 [14] and CO_2 [15]. Much attention was recently paid to the cristobalite-like ternary oxides. The partially collapsed cristobalite structures were found for the silica analogues BPO_4, $BAsO_4$ [16, 17] and phosphorus oxynitride PON [18].

In the beginning of 90^{th} analogous cristobalite-like filled structures were reported for cristobalite-like germanates [19] and titanates [20]. It was also found that some representatives of this family exhibit a high-temperature ferroelectric behavior [20]. Other filled cristobalite-like FWS possess an outstanding ionic conductivity [21]. A rich variety of filled and unfilled cristobalite-like compounds was considered in Ref [22].

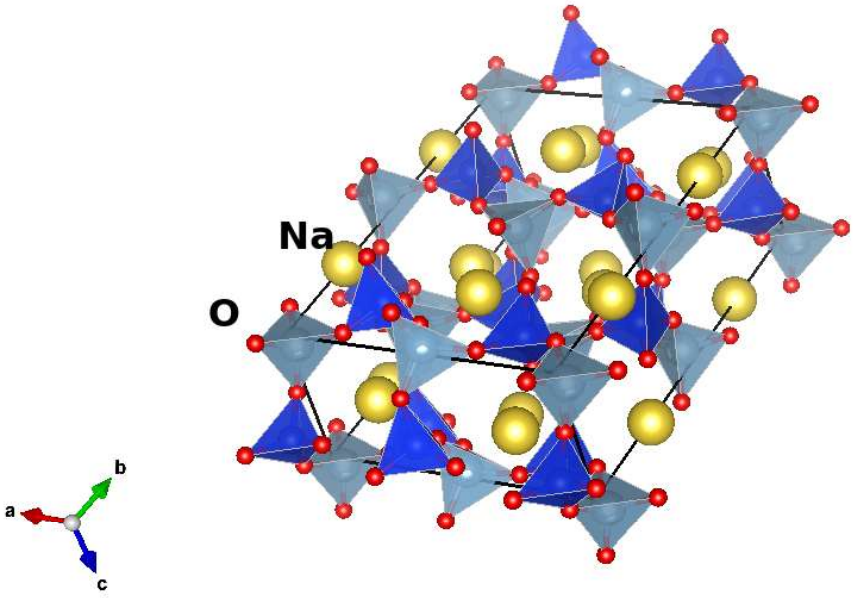

Figure 2: Example of "filled" or "stuffed" cristobalite derivative structure (carnegieite $NaAlSiO_4$)

This case corresponds to line 8 in table 1, with space group #29, setting *Pb*2_1*a.* The orientation is chosen to facilitate comparison with Figure 1. SiO_4 are darker tetrahedra, lighter are AlO_4 tetrahedra (from data of ref. [13])

Structural patterns of the structures listed in Table 1 allow a suggestion that all of them can be considered as distorted C9 aristotype structure and that the distortions do not break the connectivity of the tetrahedral framework. The question is if all the distortions can be represented within a unified basis set. In order to answer this question we consider the whole spectrum of the RUM in the C9 lattice.

The present article expounds application of the MLRUM concept, advanced in the preceding chapter [23], to the analysis of structural variety within the cristobalite family.

II. RUMs in β-cristobalite

The RUMs in β-cristobalite were first studied in Ref [24]. A specific feature of the structure is the presence of entire planes in k-space in which the RUMs exist [24]. Let us denote them as RUM-planes. To describe them, let us consider the Brillouin Zone

(BZ) shown in Fig. 3. One of the RUM-planes which pass though X-L-K points is indicated by dashed lines.

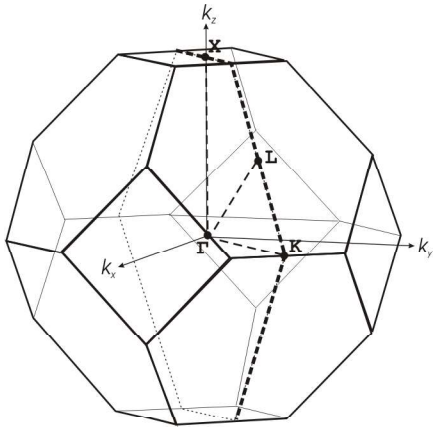

Figure 3: Special points in BZ of β-cristabolite

X, L, and K type points are shown in Figure 3. One of the RUM-planes which pass though X-L-K points is indicated by dashed lines. There are six such plans in the BZ. One can see that the Γ-X line belongs to two RUM-planes, the Γ-L line belongs to three RUM-planes, and only one RUM-plane passes through the Γ-K line. In order to visualize the atomistic pattern of the RUMs, let us consider the RUM branch in the Γ-K-X direction (along the $(\xi\xi 0)$ line in BZ). There is only one RUM in this direction, and the degeneracy problem is avoided. Fig. 4 shows eigenvectors of the RUMs belonging to **k** = (000), (¼¼0) and (½½0).

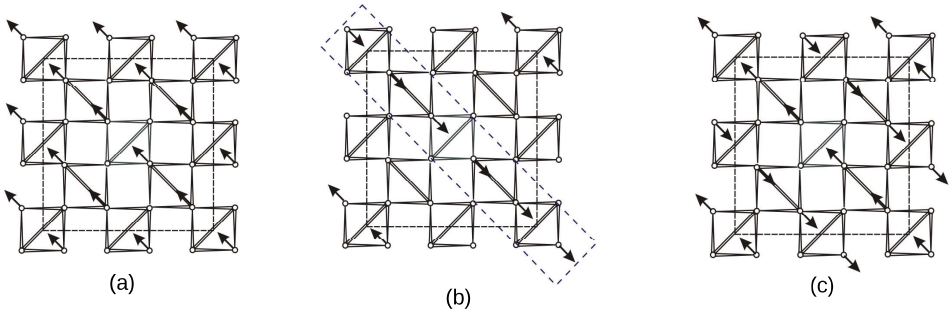

Figure 4: Atomic displacements for the RUMs with k = (000) (a), k = (¼¼0) (b), k = (½½0) (c). Crystal structure is viewed in (001) direction.

One can see that in all these modes only a half of the O atoms oscillate. In the gross, these modes involve the vibrations localized within the one-tetrahedron layers (one

such layer is displayed by the blue dashed rectangle in Fig 4b), and these vibrations are modulated in the **k**=(ξξ0) direction according to the $\exp(2\pi i\xi)$ law.

Now let us look at the RUM branch along the Γ-X direction (along the (00ζ) line). There are two RUM branches in this direction. To avoid the degeneracy problem we start with the Γ-point RUM shown in Fig. 4a and trace its evolution along the (00ζ) direction.

Fig. 5 shows eigenvectors of the RUMs with k = (000), (00¼) and (00½). The structures shown in Fig. 5 are viewed in the (110) direction.

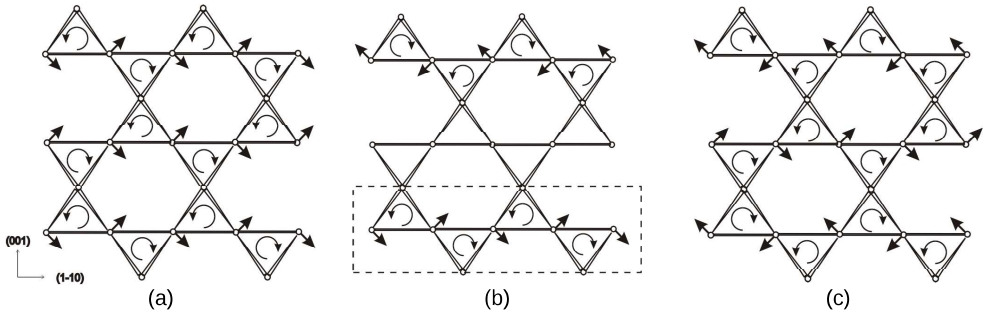

Figure 5: Atomic displacements for the RUMs with k = (000) (a), k = (00¼) (b), k = (00½) (c) Crystal structure is viewed in (110) direction.

One can see the same situation: only a half of the O atoms oscillate in all these modes. These modes involve vibrations localized within the one-tetrahedron layers (one such layer is highlighted in Fig. 5b by the blue rectangle), and these vibrations are modulated in the **k**=(00ζ) direction according to the $\exp(2\pi i\zeta)$ law.

Intersection of the one-tetrahedron layers highlighted in Figs. 4b and 5b contains one infinite chain extended in the $(1\,1\,0)$ direction. The modes shown in Figs. 4 and 5 can be considered as different combinations of the in-chain localized vibrations. Below we shall refer such vibrations as Chain Tilting Mode (CTM). One of CTM is shown in Fig. 6. The existence of CTM is a particular feature of the C9 lattice. The tetrahedra forming the chain may concordantly rotate without perturbing the rest of the lattice.

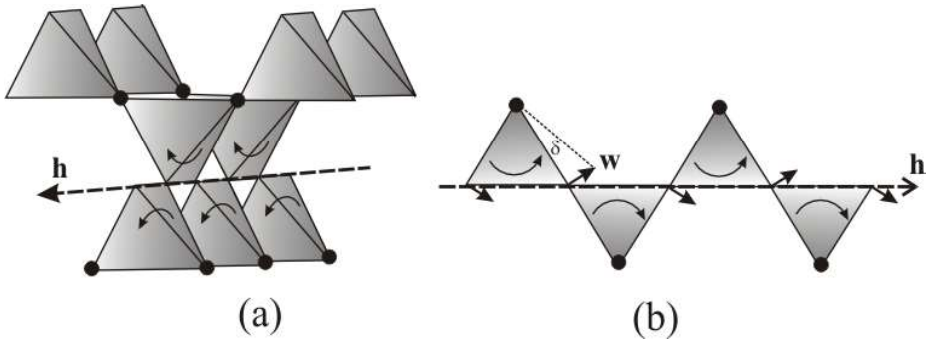

Figure 6: Atomistic pattern of CTM.

Tetrahedron rotations are shown by curvy arrows. The immovable atoms are shown by solid circles. The atomic displacements are shown by arrows **w** in panel (b). Vector **h** indicates the chain direction.

Every CRM can be characterized by the chain direction vector **h** and the rotational angle δ. Atomic displacements of atoms forming the chain (vectors **w**) are shown in Fig 6b. Their amplitude is related with rotational angle as

$$|w| = \frac{a}{4}\sqrt{\frac{3}{2}}\delta \ . \qquad (1)$$

Note that CTM are analogous to the “coupled tetrahedral edge rotations” considered in Ref [25].

III. Maximally localized RUMs in cristobalite

If we look at the C9 structure along the $(1\,1\,0)$ direction we can easily discern the chains stretched in the $(1\,1\,0)$ direction. If we designate the in-chain localized distortions by spin-like arrows, the picture can be represented as shown in Fig. 7. Denote the chain position by vector **R** and the amplitude of in-chain distortion as $w(\mathbf{R})$. The eigenvector of the RUM corresponding to arbitrary **k**-vector in the plane $(\xi\xi\zeta)$ plane can be determined by the expression:

$$e(\mathbf{k}) = \sum_{\mathbf{R}} e^{i\mathbf{k}\cdot\mathbf{R}} w(\mathbf{R}) \qquad (2)$$

The RUMs presented in Figs. 4 and 5 also obey the Eq (2) with **k**-vectors indicated under the figures.

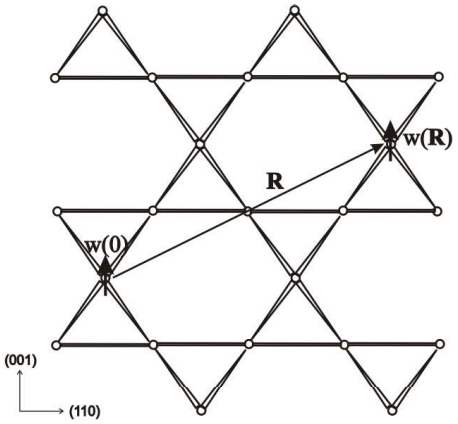

Figure 7: Schematic picture of RUMs localized in the chains extended along the $(1\,1\,0)$ direction. The structure is viewed along the $(1\,1\,0)$ direction.

It is noticeable, that the Eq. (2) coincides with the expression which relates the Bloch functions *e*(**k**) and the Wannier functions *w*(**R**) in the electronic band theory [26]. The inverse relation is:

$$w(R)=\frac{V}{(2\pi)^3}\int_{BZ} dk\, e^{-ik\cdot R} e(k) \qquad (3)$$

As is well known, the Bloch functions and consequently the Wannier functions are not unique. In the electronic band theory, several routines were proposed to select, from among the many arbitrary choices of Wannier functions, the particular set that is maximally localized [26, 27]. Our experience shows that the problem of ambiguity of the Wannier functions is not daunting in the case of the RUM vibrations. The use of the Eq (3) allows us to determine the localized RUM which cannot be contracted anymore. In the case of cristobalite, Eq (3) provides us with an exact analytic definition of the in-chain localized RUM, i.e. CTM. It can be shown that thus defined *w*(**R**) phonon mode is the Maximally Localized Wannier Mode (MLWM) for the RUM branch in the $(\xi\xi\zeta)$ plane of reciprocal space.

The CTM concept allows us to describe arbitrary RUM at arbitrary k-point as a combination of the CTM. This provides us with a basis for unified classification of the whole RUM spectrum and allows an uniform classification of the collapsed structures induced by the RUM condensation.

Any tetrahedron has six edges. Accordingly, there are six linear chains involving the tetrahedron in the C9 lattice. Let us introduce six chain vectors $\mathbf{h}_i$ (i=1,.., 6) directed along the chains and normalized according to the expression

$$|h_i| = 2\sqrt{2}\pi/a \qquad (4)$$

Such a normalization preserves the periodicity of the CTM along the chain. The chain vectors are shown in Fig. 8 and are listed in Table 2.

Table 2: Definition of the chain vectors $\mathbf{h}_i$

i	1	2	3	4	5	6
$\frac{a}{2\pi}h_i$	(110)	$(1\,1\,0)$	(101)	$(1\,0\,1)$	(011)	$(0\,1\,1)$
Chain vectors	$\mathbf{a}_2$	$\mathbf{a}_1$ - $\mathbf{a}_3$	$\mathbf{a}_1$	$\mathbf{a}_2$ - $\mathbf{a}_3$	$\mathbf{a}_3$	$\mathbf{a}_2$ - $\mathbf{a}_1$
Apexes	(12)	(34)	(41)	(23)	(31)	(24)

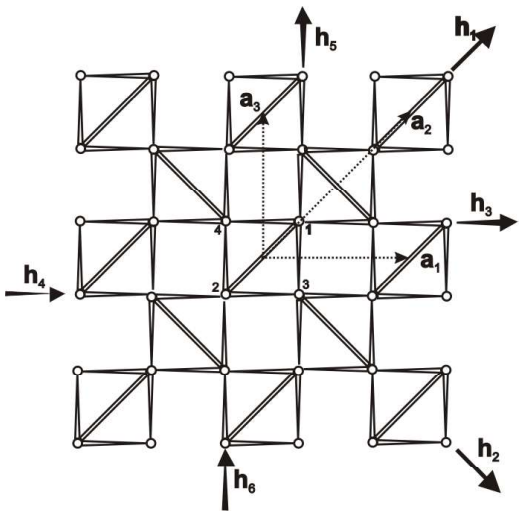

Figure 8: Chain vectors $\mathbf{h}_i$ and primitive cell vectors $\mathbf{a}_1 = (\frac{1}{2}\,0\,\frac{1}{2})a$, $\mathbf{a}_2 = (\frac{1}{2}\,\frac{1}{2}\,0)a$, $\mathbf{a}_3 = (0\,\frac{1}{2}\,\frac{1}{2})a$

For brevity and for better visualization we shall refer the h-vectors listed in Table 2 by specifying a couple of the apexes indicated in the central tetrahedron:

The RUM related to the one-chain CTM can be characterized by specifying following parameters :

h-vector which determines the chain direction,
$\mathbf{s}_1$ and $\mathbf{s}_2$ – two vectors non-collinear with **h**,
ϕ_1 and ϕ_2 phase shifts CTM in the $\mathbf{s}_1$ and $\mathbf{s}_2$ directions.

Then atomic displacement of the tetrahedron located in **R**-site are determined by the expression

$$w(\mathbf{R}) = w_0(\mathbf{h}) \exp\left[i\phi_1(\mathbf{R} \cdot \mathbf{s}_1) + i\phi_2(\mathbf{R} \cdot \mathbf{s}_2) \right] \quad (5)$$

Atomic displacements determined by arbitrary combination of the expressions (3) would correspond of a RUM.

The concept of CTM can be used to describe the RUM branches along special k-directions. According to Eq. (1), any k-direction non-collinear with the given chain direction contains one RUM branch related to this CTM. Hence, in order to determine the RUM states for a given k-direction one must indicate the CTMs non-collinear with this direction, e.g. the h-vectors perpendicular to the k-direction. Results of such analysis for the symmetric k-directions are shown in Table 3.

Table 3: The h-vectors perpendicular to special k-directions and number of RUMs along the directions (N_r).

k-directions	**h**⊥**k**	N_r
k=$(\xi 00)$	$\mathbf{h}_5$, $\mathbf{h}_6$	2
k=$(\xi\xi 0)$	$\mathbf{h}_2$	1
k=$(\xi\xi\xi)$	$\mathbf{h}_2$, $\mathbf{h}_6$, $\mathbf{h}_4$	3
k=$(\xi\xi\zeta)$	$\mathbf{h}_2$	1

One can see that N_r values determined from analysis of CTM coincide with numbers of RUM branches derived from lattice dynamics calculations [6].

To summarize, the results presented in this section show that the CTM concept not only allows us to count the number of RUMs for arbitrary k-point but also to visualize their atomistic patterns.

IV. Collapsed crystal structures induced by CTM condensation

In the preceding section we have established the unified scheme for representing arbitrary RUM as combination of the CTMs. Hence, by constructing various combinations of the CTM and considering the correspondingly distorted C9 structures, one can describe the infinite variety of the cristobalite-like collapsed structures – commensurate and incommensurate ones as well. In this paper we show that the approach allows us to describe in a uniform manner all known cristobalite-like structures listed in Table 1.

Our procedure was as follows. We took the experimentally determined unit cell vectors **a**(R) and atomic positions **x**(R) in the structure under study. Through the analysis of **a**(R), we determined its relation with the unit cell of C9 structure $\mathbf{a}_0$ that defines the transformation matrices A:

$$\mathbf{a}(\mathrm{R}) = \mathbf{A}\mathbf{a}_0 \qquad (6)$$

The A-matrixes are listed in Table 3.

Table 3: Transformation matrixes and unit cell multiplication number Z for the known cristobalite-like structures.

#227	*Fd*3*m*	Z=2	$\begin{pmatrix} 1 & 0 & 1 \\ 1 & 1 & 0 \\ 0 & 1 & 1 \end{pmatrix}$	#14	$P2_1/c$	Z=8	$\begin{pmatrix} -1 & -1 & 2 \\ 1 & -1 & 0 \\ 2 & 2 & 0 \end{pmatrix}$
#122	$I42d$	Z=2	$\begin{pmatrix} 1 & 1 & 0 \\ -1 & 1 & 0 \\ 0 & 1 & 1 \end{pmatrix}$	#33	$Pna2_1$	Z=4	$\begin{pmatrix} 1 & 1 & 0 \\ -1 & 1 & 0 \\ 0 & 0 & 2 \end{pmatrix}$
#92	$P4_12_12$	Z=4	$\begin{pmatrix} 1 & 0 & 1 \\ -1 & 1 & 0 \\ 0 & 0 & 2 \end{pmatrix}$	#61	*Pbca*	Z=16	$\begin{pmatrix} 1 & 1 & 0 \\ -2 & 2 & 0 \\ 0 & 0 & 4 \end{pmatrix}$
#198	$P2_13$	Z=8	$\begin{pmatrix} 2 & 0 & 0 \\ 0 & 2 & 0 \\ 0 & 0 & 2 \end{pmatrix}$	#29	$Pb2_1a$	Z=16	$\begin{pmatrix} 2 & 2 & 0 \\ -1 & 1 & 0 \\ 0 & 0 & 4 \end{pmatrix}$

Table 4: Representation of known collapsed cristobalite structures as combinations of CTM distortions

SG	CTM combinations			
	$\mathbf{h}_m$	δ_m	$\mathbf{s}_1$, ϕ_1	$\mathbf{s}_2$, ϕ_2
#92	(12)	δ_0	(13), π	(14), π
	(34)	δ_0	(13), π	(32), π
#122	(12)	δ_0	(13), 0	(14), 0
	(34)	δ_0	(13), 0	(32), 0
#198	(14)	δ_0	(13), π	(12), π
	(23)	δ_0	(13), π	(12), π
	(12)	δ_0	(13), π	(14), π
	(34)	δ_0	(13), π	(14), π
	(13)	δ_0	(12), π	(14), π
	(42)	δ_0	(12), π	(23), π
#14	(12)	δ_1	(13), π	(14), π
	(34)	δ_2	(12), π	(001), π
#33	(12)	δ_1	(13), π	(14), π
	(34)	δ_2	(13), 0	(14), 0
#61	(12)	δ_1	(34), 0	(24), π/2
	(34)	δ_2	(12), π	(001), 0
#29	(12)	δ_1	(34), 0	(001), π
	(34)	δ_2	(12), π	(001), 0

Thereupon we have represented the C9 structure in the crystallographic setting of the structure under study. Thus the atomic positions in the undistorted structure **x**(0) were determined. The atomic positions **x**(R) and **x**(0) are listed in the Attachment. The data collected in Tables A1-A7 show that atomic positions for all collapsed structures are close to those of the corresponding aristotype structure with only one exception – the *y*(Si2) parameter in the #14 structure. If one neglects this particularity of the cristobalite-II structure the average deviation will be about 0.04 – a little bit larger than the experimental inaccuracy. The unit cell parameters of the collapsed structures also agree well with the values obtained for corresponding supercells of the aristotype structure with average *a* parameter close to 7 Å.

The problem was to fit the displacement vectors $\delta\mathbf{x} = \mathbf{x}(R) - \mathbf{x}(0)$ by a linear combination of the CTM-distortions. It was solved as follows. The whole set of CTM

within the extended unit cell coincides with the set h-vectors passing through the cell. Denote such h-vectors as $\mathbf{h}_m$ $(m = 1,...,M)$. Using the atomistic pattern of CTM defined by Fig. 6 and Eq. 1 we have constructed the set of CTM-distortions which are characterized by their amplitudes δ_m. These quantities are coefficients of the linear combination and are determined by the use of the least-square method. The CTMs which give maximal contributions to the $\delta\mathbf{x}$ vectors are represented in Table 4. They can be considered as minimal CTM distortions which transform the C9 structure to the structure in hand.

V. Concluding remarks

As demonstrated in this study, the structural particularity of the β-cristobalite lattice gives rise to ***Chain Tilting Modes*** (CTMs) which are the ***Rigid Unit Modes*** (RUMs) localized within linear chains running in six crystallographic directions.

An important result is that any RUM in the β-cristobalite can be represented by a proper combination of several CTMs.

It is remarkable that all distorted cristobalite-like crystal structures can be represented as resulting from joint condensation of several CTMs. This conclusion is approved by the analysis of all reported cristobalite-like structures.

The concept of CTM is of high interest as it offers a direct and universal way to construct the transformation paths for structural transformations and to model the domain wall structure in cristobalite-type materials having a polydomain texture.

Complementary informations on authors:

e-mails: smirnomb@rambler.ru and pstgregoire@gmail.com

Cite this paper: M.B. Smirnov and P. Saint-Gregoire, OAJ materials and Devices, vol 5(1) – chap No11 in "Perovskites and other Framework Structure Crystalline Materials", p 355 (Coll. Acad. 2021) - DOI:10.23647-ca.md20202205

REFERENCES

1. Wyckoff R.W.G., Zeitschrift für Kristallographie, **62,** 189 (1925)

2. Peacor D. R., Zeitschrift für Kristallographie, **138**, 274 (1973)
3. Barth T.F.W., *Am. J. Sci.,* **24,** 97 (1932)
4. Nieuwenkamp W., Zeitschrift für Kristallographie, **92**, 82 (1935)
5. Wright A.F., A.J.Leadbetter, *Phil. Mag*. **31** 1391 (1975)
6. Dollase W.A., Zeitschrift für Kristallographie **121**, 369 (1965)
7. Hatch D.M., S.Ghose, *Phys. Chem. Minerals,* **17**, 554 (1991)
8. D.C.Palmer, L.W. Finger, *Amer. Mineral.* **79**,1 (1994)
9. M.T.Dove, M.S.Craig, D.A.Keen, W.G.Marshall, S.A.T.Redfern, K.O.Trachenko, M.G.Tucker. *Mineralogical Magazine* **64**, 569 (2000)
10. Barth T.F.W., *J. Chem. Phys*. **3**, 323 (1935)
11. M.J.Buerger, *Amer. Mineral.* **39**, 600 (1954)
12. E.Vielhaber, R.Hoppe, *Z. Anorg. Allgem. Chem.* **369**, 14 (1969)
13. R.L.Withers, J.G.Thompson, *Acta Crystallogr*. **B49**, 614 (1993)
14. H.Bohm, *Naturwissenschaften* **55**, 648 (1968)
15. M.Santoro, F.A.Gorelli, R.Bini, J.Haines, O.Cambon, C.Levelut, Jr.A.Montoya, S.Scandolo, *Proc. Nat. Acad. Sci. USA* **109** 5176 (2012)
16. K.Kosten, H.Arnold. *Z. Kristallogr.* **152**, 119 (1980)
17. J.Haines, C.Chateau, J. M.Leger, C.Bogicevic, S.Hull, D. D.Klug, J.S.Tse, *Phys. Rev. Letters* **91**, 015503 (2003)
18. J.M.Léger, J.Haines, C.Chateau, G.Bocquillon, M.W.Schmidt, S.Hull, F.Gorelli, A.Lesauze, R.Marchand, *Phys. Chem. Miner.* **28**, 388 (2001)
19. J.Grins, D.Louer, *J. Solid State Chem*. **87**, 114 (1990)
20. C.Colbeau-Justin, A.Elfakir, M.Quarton, *Ferroelectrics*, **185**,157 (1996)
21. A.Jones. *Ionic Mobility In Filled-Silica Minerals*. PhD thesis. The Open University UK (2000). https://oro.open.ac.uk/19720/1/pdf49.pdf
22. M.O'Keefe, B.G.Hyde, *Acta Cryst*. **B32**, 2923 (1976)
23. Smirnov M.B. and P. Saint-Gregoire, OAJ Materials and Devices, vol. 5 (1), 150120 (2020) – DOI: 10.23647/ca.md20201501
24. I.P.Swainson, M.T.Dove, *Phys. Rev. Lett*. **71**, 193 (1993)
25. R.L.Withers, C.Lobo, J.G.Thompson, S.Schmid, R.Stranger, *Acta Cryst.* **B53**, 203 (1997)
26. N.Marzari, D.Vanderbilt. *Phys. Rev*. **B56**, 12847 (1997)
27. G. Berghold, C. J. Mundy, A.H. Romero, J. Hutter, and M. Parrinello *Phys. Rev.* **B61**, 10040 (2000)

Appendix:

Experimentally determined structural parameters for different cristobalite-like structures and their relations with those of the aristotype C9 structure

Table A1. Structural parameters for #122 structure of SiO_2

	exp [4]			aristotype		
a,b, c	5.042	5.042	7.131	$a/\sqrt{2}$	$a/\sqrt{2}$	a^*
Si	0	0	0	0	0	0
O	0.079	0.25	0.125	0	0.25	0.125

*) here and below *a* is the unit cell parameter of the C9 structure

Table A2: Structural parameters for #92 structure of SiO_2

	exp [6]			aristotype		
a,b,c	4.978	4.978	6.948	$a/\sqrt{2}$	$a/\sqrt{2}$	*a*
Si	0.3000	0.3000	0.0000	.25	.25	0
O	0.2398	0.1032	0.1784	.25	.0	.125

Table A3: Structural parameters for #198 structure of SiO_2

	exp [3]			aristotype		
a,b,c	7.16	7.16	7.16	*a*	*a*	*a*
Si1	0.255	0.255	0.255	0.25	0.25	0.25
Si2	-0.008	-0.008	-0.008	0	0	0
O1	0.125	0.125	0.125	0.125	0.125	0.125
O2	0.660	0.660	0.062	0.625	0.625	0

Table A4: Structural parameters for #14 structure of SiO_2

	exp [9], β=124.939°			aristotype, β= $\arccos(-1/\sqrt{3}) = 125.3°$		
a,b,c	8.3769	4.6020	9.0583	$a\sqrt{3}/2$	$a/\sqrt{2}$	$a\sqrt{2}$
Si1	0.3725	0.2310	0.2145	0.375	0.25	0.1875
Si2	0.1207	0.4699	0.8403	0.125	0.25	0.8125
O1	0.1859	0.3645	0.0351	0.25	0.25	0
O2	0.2997	0.0912	0.3276	0.25	0.25	0.25
O3	0.5296	0.4791	0.3297	0.5	0.5	0.25
O4	-0.073	0.3089	0.6839	0	0.5	0.75

Table A5: Structural parameters for #33 structure of $NaGaO_2$

	exp [12]			aristotype		
a,b,c	5.301	5.519	7.201	$a/\sqrt{2}$	$a/\sqrt{2}$	*a*
Ga	0.000	0.061	0.123	0	0	0.125
O1	0.064	0.395	0.173	0	0.25	0.25
O2	0.672	0.060	0.102	0.75	0	0

Table A6: Structural parameters for #61 structure of $KGaO_2$

	exp [12]			aristotype		
a,b,c	5.51	11.07	15.81	$a/\sqrt{2}$	$a\sqrt{2}$	2*a*
Ga1	0.261	0.008	0.189	0.25	0	0.1875
Ga2	0.280	0.264	0.065	0.25	0.25	0.0625
O1	0.574	0.296	0.013	0.5	0.25	0
O2	0.153	0.402	0.106	0.25	0.375	0.125
O3	0.306	0.174	0.155	0.25	0.125	0.125
O4	0.925	0.486	0.225	0	0.5	0.25

Table A7: Structural parameters for #29 structure of $NaAlSiO_4$

	exp [13]			aristotype		
a,b, c	10.261	5.156	14.030	$a\sqrt{2}$	$a/\sqrt{2}$	2*a*
Al1	0.034	0.067	0	0	0	0
Al2	0.282	0.441	0.246	0.25	0.5	0.25
Si3	0.716	0.064	0.371	0.75	0	0.375
Si4	0.032	0.563	0.125	0	0.5	0.125
O1	0.067	0.001	0.403	0.125	0	0.4375
O2	0.446	0.498	0.220	0.625	0.5	0.1875
O3	0.498	0.143	0.095	0.5	0.25	0.0625
O4	0.249	0.637	0.347	0.25	0.75	0.3125
O5	0.306	0.002	0.464	0.375	0	0.4375
O6	0.183	0.497	0.148	0.375	0.5	0.1875
O7	0.003	0.389	0.032	0	0.25	0.0625
O8	0.246	0.123	0.283	0.375	0.25	0.3125

Chapter 12 : Amorphous materials based on perovskite ferroelectrics

S.A. Gridnev (1), L.N. Korotkov (2)

(1) Professor, Voronezh State Technical University, Russia
(2) Professor, Voronezh State Technical University, Russia

Corresponding author: l_korotkov@mail.ru

Abstract : The methods of preparation, as well as the structure and most relevant physical properties of amorphous materials based on ferroelectrics with perovskite structure are reviewed. The theoretical basis for the possibility of ferroelectricity in non-crystalline solids is discussed. The structural relaxation in a glassy state and the crystallization processes leading to the formation of a ferroelectric phase are considered. The structure and physical properties of thin-film amorphous ferroelectrics that demonstrate noticeable differences from the properties of the same materials in bulk state are discussed separately.

Keywords : AMORPHOUS FERROELECTRICS, THEORETICAL PREDICTIONS, PREPARATION METHODS, STRUCTURE, DIELECTRIC PROPERTIES, CRYSTALLIZATION KINETICS

Cite this paper: S.A. Gridnev and L.N. Korotkov, OAJ materials and Devices, vol 5(1) – chap No12 in "Perovskites and other Framework Structure Crystalline Materials", p373 (Coll. Acad. 2021) DOI:10.23647/ca.md20202808